Direct nanoscale imaging of ballistic and diffusive thermal transport in graphene nanostructures

Manuel E. Pumarol[1], Mark C. Rosamond[2], Peter Tovee[1], Michael C. Petty[2], Dagou A. Zeze[2], Vladimir Falko[1], and Oleg V. Kolosov[1*]

[1]Physics Department, Lancaster University, Lancaster, LA1 4YB, UK,
[2]School of Engineering & Computing Sciences, Durham University, Durham DH1 3LE, UK.

ABSTRACT We report direct imaging of nanoscale thermal transport in single and few-layer graphene with approximately 50 nm lateral resolution using high vacuum scanning thermal microscopy. We observed increased heat transport in suspended graphene where heat is conducted by ballistic phonons, compared to adjacent areas of supported graphene, and observed decreasing thermal conductance of supported graphene with increased layer number. Our nanothermal images suggest a mean-free-path of thermal phonons in supported graphene below 100 nm.

KEYWORDS Nanoscale thermal transport, nanoscale imaging, ballistic phonons, thermal conductivity, graphene, Scanning Thermal Microscopy.

The list of graphene properties showing potential for nano-electronics applications includes high carrier mobility, superior mechanical strength - and high thermal conductivity.[1-3] While graphene electronic properties have been extensively studied at scales ranging from micrometre down to nanometre, the nanometre length scale investigation of heat transfer in graphene nanostructures is still a largely unexplored area. Findings reported to date point to the extraordinary thermal properties of graphene as a two-dimensional (2D) nanomaterial,[4-9,10] suggesting that supported and free-standing films of graphene can be used for heat management in nanoscale devices. With the mean-free-path (MFP) of thermal phonons at room temperature in graphene estimated to be in the order of 250-800 nm[6,11, 12] and the typical feature size of modern electronic devices in the order of a few tens of nm, it is apparent that the ballistic regime must play a significant role in thermal transport in graphene-based nanodevices[13]. This highlights the importance of exploration of heat generation and transport in such devices with nanoscale spatial resolution. So far that was not possible, as these phenomena have been studied either in stationary devices[9, 14] in experiments using micro-Raman spectroscopy, with lateral resolution inevitably restricted by the optical wavelength to the range of 0.5 - 1 μm[4,6] - and relatively low temperature sensitivity.

In this Letter we address the challenge of exploring thermal phenomena in graphene nanostructures by using a nanoscale scanning thermal probe in a high vacuum (HV) environment that allowed us to directly map thermal transport in suspended and supported graphene layers with nanoscale resolution, and to explore both ballistic and diffusive regimes of heat transfer. We compare measured thermal resistance measurements R_c of a SiO_2 tip-graphene thermal junction for different number of graphene layers and for a suspended *vs.* supported bi-layer on a 180 nm wide channel (Fig. 1a) where ballistic transport effects can be directly observed. We also perform a theoretical calculation of the MFP of phonons on

* To whom correspondence should be addressed. E-mail: o.kolosov@lancaster.ac.uk, http://www.nano-science.com.

supported graphene. This find is further supported by profile thermal maps measured at inter-layer boundaries.

The thermal conductivity of graphene sheet materials, *k,* has the highest known value in nature, both theoretically predicted, 6600 W/mK for an isolated unzipped carbon nanotube graphene layer[15], and experimentally measured, 5300 W/m-K for μm sized flakes of suspended single-layer graphene (SLG).[8] In thin graphene layers, the relative value of contribution to total heat conductivity between out-of-plane flexural phonons (ZA), and in-plane transverse (TA) and longitudinal acoustic acoustic (LA) phonons depends on the complex interplay[10] between phonon density of states (favoring ZA phonons), group velocity (higher for LA and TA phonons)[16] as well as higher order nonlinearities[17]. The size dependent heat conduction in 2D systems also should be taken into account[10]. In view of current knowledge[10, 17] it is reasonable to consider that all acoustic modes contribute to approximately similar extent to the heat conductivity in suspended graphene at room temperature, with ZA contribution decreasing with the temperature increase, and electrons in un-doped graphene contributing less than 1%[8,9,10].

Previous measurements of heat transport investigated diffusive thermal transport regime either using fixed 'thermal bridge' configuration[9] for graphene in contact with supporting substrate and yielded *k* of 600 W/mK, or used innovative optical Raman measurements.[6,8,18].This last value is an order of magnitude lower than for suspended graphene, suggesting that heat transport by all acoustic phonons in supported graphene is suppressed by interaction with the substrate, with out-of-plane ZA phonons contribution affected the most[17].

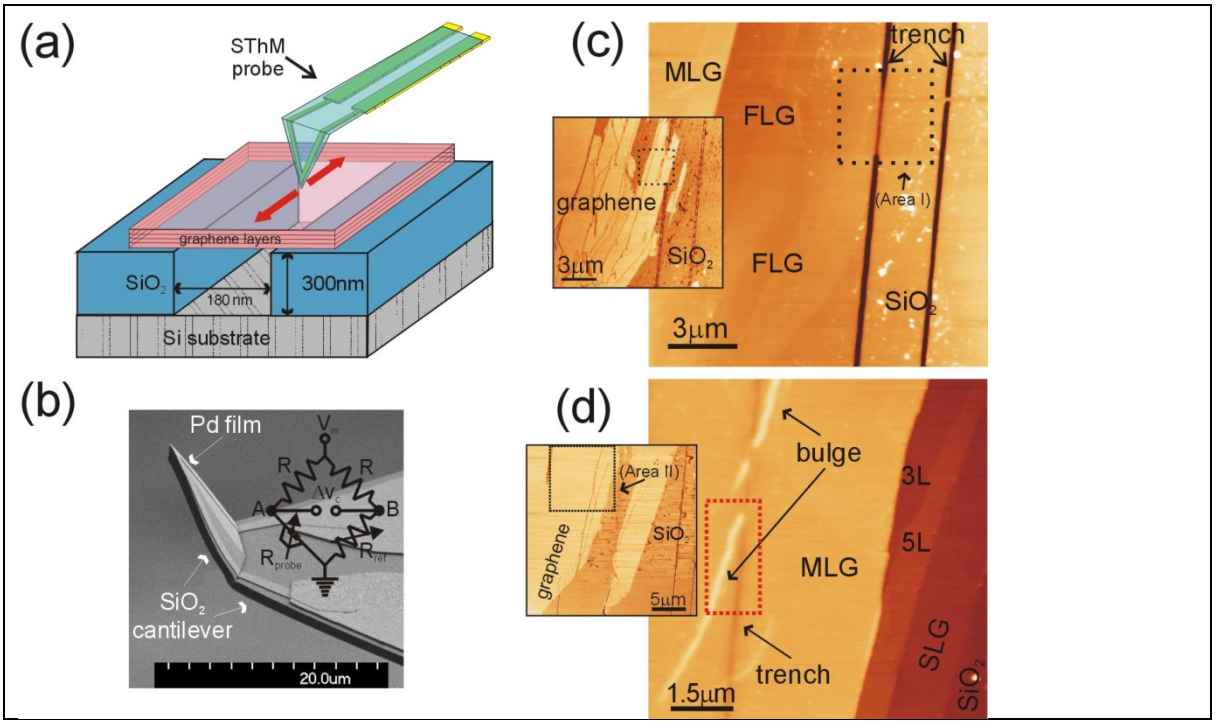

Figure 1 (a) Schematic diagram of the graphene sample on trench substrate, with SThM tip in a typical experimental configuration. (**b)** SEM image of the SThM probe (courtesy of Anasys Instruments); embedded, a schematic diagram of the circuitry used for heating and temperature measurement of the nanoscale SThM probe. The driving signal V_{in} is a composite DC (heating) + AC (temperature probing) signal. (**c**), (**d)** AFM topography scan showing the different heights of the graphene layers. The main body of the flake was about 17 atomic layers thick, with few-layer graphene (FLG) regions (from SLG up to 5- layer FLG) to the right side of the flake. An area of interest of a suspended BLG sheet is enclosed in the dotted square. The insets show a friction force map of the same areas, which allowed clear identification of graphene and silicon oxide surfaces during SThM measurements owing to clear difference between these areas in friction contrast.

In the present study, to investigate nanoscale graphene thermal properties, the graphene samples were prepared by mechanical micro-cleavage exfoliation of graphite[1, 3, 19] followed by deposition onto Si/SiO_2 substrates which have pre-patterned sharp trenches of 180 nm wide and 300 nm deep. The test samples consisted of suspended and supported sheets of single, double, and multilayer graphene. The presence, number of layers, and location of graphene was determined by Raman,[20] optical contrast,[6, 21, 22] bi-directional topography, and friction atomic force microscopy (AFM) measurements. Micro-Raman and optical contrast were used for identifying relatively wide 1 to 3 layer graphene areas, that subsequently were used as a base reference for z-calibrated AFM topography for identifying thickness of thin and thick multi-layer graphene. Suspension of graphene over the trench and in delaminated areas was confirmed by AFM contact compliance measurements [23]. Edge lithography was used to define trenches on the oxidized silicon substrate surface.[24]

For thermal transport measurement we developed a specialised HV (pressure ~ 10^{-7} torr) Scanning Thermal Probe Microscope[25, 26] (SThM) that uses a microfabricated thermal sensor on a force sensitive cantilever, see Fig. 1b. The setup allowed us to map locally the heat flow into the sample with a lateral resolution of approximately 50 nm, providing an order of magnitude better spatial resolution for thermal transport in graphene than previously reported.[4, 6]

During measurements the SThM sensor was heated by a constant power Joule heating and as the probe was scanned in a raster way across the sample at a constant force, the sensor temperature was monitored, producing SThM maps. The SThM was based on a microfabricated resistive probe[27, 28] from Anasys Instruments (EXP-GLAI) and consists of a heater-temperature sensor probe with metallic resistive layer of 5 nm NiCr and 40 nm Pd deposited on top of a 1 μm thick SiO_2 cantilever. SThM scans were performed using standard AFM force feedback at constant force which allowed us to maintain uniformity of thermal contact between the tip and the sample. The probe thermal resistance, in vacuum, when the tip is out of contact R_{PO}, was taken as a reference value. When the probe was brought into contact with the sample, a solid-solid heat conduction channel with thermal resistance R_C (which is linked to the heat transport in a probed material) is opened and as a result a sudden change of the probe temperature is observed. This change is only about 2 to 3% of the temperature difference between the heater and the sample, and due to high SThM tip apex thermal resistance, the temperature of the probed material in immediate contact with the probe is much less than that of the heater.

The measured total thermal resistance of the probe R_P in contact with the surface R_{PI}, is a parallel combination of R_{PO} and R_C, and can be obtained by solving the parallel thermal circuit, namely

$$\frac{1}{R_{\mathrm{PI}}} = \frac{1}{R_{\mathrm{PO}}} + \frac{1}{R_{\mathrm{C}}}. \qquad [1]$$

Ultimately, the contact thermal resistance can be represented as the sum of the tip-graphene junction resistance R_j and the graphene sheet thermal resistances R_G where $R_C = R_j + R_G$. The junction resistance is dependent on the geometry and thermal conductance of the SThM tip apex as well as nature of the contacting surfaces, that is sensitive to the contact area between tip and sample.[29] Since the same SThM tip was used for all our measurements, the contacting surfaces had the same dimensions and physical nature (tip-graphene contact), and thermal resistance was observed to be independent of the applied normal force up to 100 nN (with forces used in our measurements were well below 10 nN), then R_j could be safely treated as a constant. The range of values of R_j can be determined from the thermal conductance per unit of area for a graphene-silicon oxide and graphene-metal interfaces that was reported to be in the range from 85 x 10^6 to 120 x 10^6 W/m^{2}K (±20%) and independent on the number of graphene layers.[30] For the 50x50 nm^2 contact area that would result in thermal resistance between 2 to 4 x 10^6 K/W comparing well with our range of measured thermal resistances around 3x10^6 ± 3x10^4 K/W. Furthermore, as shown elsewhere,[31] another component of R_j is the SThM end-of tip resistance that as we confirm in our finite element analysis significantly exceeds R_G. Therefore, by approximating the graphene thermal resistance of the thick and highly thermally conductive 17-layer supported graphene $R_{G(17L)}$ as zero, an upper end estimate of junction resistance $R_j = R_{C(17L)} = 2.57\text{x}10^6 \pm 3\text{x}10^4$ K/W is obtained. This allowed us to directly estimate link graphene sheet thermal resistance with changes in thermal resistances R_{PI}, R_{PO} that are measured with the SThM setup:

$$R_G \approx \frac{R_{PI} R_{PO}}{R_{PO} - R_{PI}} - R_{C(17L)}. \quad [2]$$

In our experiments, a lower temperature of the probe (darker contrast in SThM maps) indicates higher heat flow to the sample (therefore, a lower thermal resistance of tip-sample contact, and correspondingly, a higher thermal conductance). By calibrating the SThM sensor, we were able to calculate an estimate for intrinsic graphene sheet thermal resistance. This, in turn, allowed us to reliably compare thermal resistances for SLG, supported and suspended bi-layer graphene (BLG), and higher number of graphene layers. SThM maps (Fig. 2a) show clear differences between the thermal resistance of graphene areas with varying number of graphene layers with a spatial resolution of approximately 50 nm. The increase in the number of supported graphene layers (from SLG through 3-layer (3L) and few layer graphene, FLG) lead to a clear decrease in thermal resistance. Absolute values of total contact thermal resistances R_C, for SLG, BLG, and a trench area with suspended BLG are estimated as $R_{C(SLG)} = 3.35\text{x}10^6 \pm 3\text{x}10^4$ K/W, $R_{C(BLG)} = 3.15\text{x}10^6 \pm 3\text{x}10^4$ K/W, and $R_{C(BLG\text{-}trench)} = 2.75\text{x}10^6 \pm 3\text{x}10^4$ K/W, respectively, see Fig. 2b.

One of our key observations was that the thermal conductance of BLG layer suspended over the trench exceeded that of BLG resting on substrate (darker SThM contrast of the suspended area in Fig. 2a, SThM profiles in Fig. 2b). This finding, could be considered counterintuitive as one might expect a better heat dissipation of supported graphene where there is an additional channel of heat transfer through thin graphene layer directly to the substrate, however it suggests that a reduction of lateral heat transport in the graphene layer due to contact with substrate has a prevailing effect. As MFP of thermal phonons in suspended graphene is much larger than the distance from the centre of the trench to its border (90 nm), one can estimate (by assuming average MFP value of 600 nm[6,11,12] and symmetrical propagation of ballistic phonons in graphene plane) that approximately 90% of phonons from the apex of SThM tip will reach trench border in ballistic regime, making ballistic acoustic phonons the dominating heat escape channel in our measurement geometry. Nanoscale maps of local thermal transport in the trench area and its vicinity (Fig. 2a) support original data of diffusive thermal transport in graphene received by the Raman technique on a

wider area of suspended films,[4,6,7] while allowing direct exploration of thermal transport in graphene on a different length scale (50 nm spatial resolution in our SThM measurements *vs.* 500 – 1000 nm in Raman measurements) and correspondingly, in both ballistic and diffusive regimes of heat transfer in such systems.

In addition to the increased heat transport in thin bi-layer suspended graphene, we also observed such increases in a much thicker (~6 nm, or ~17 layers) graphene sheet suspended over the trench (Fig. 3a) that showed similar decrease of thermal resistance R_c of suspended relative to supported graphene, see SThM maps and profiles, Fig. 3b, c. Interestingly, a nearby graphene 'bulge' – an area of graphene that was out of contact with the surface– but of opposite surface curvature, also showed lower thermal resistance, see Fig. 3a, b, d. This confirms that it is the absence of contact with the substrate that increases heat transfer in a graphene sheet, and rules out possible artefacts of the SThM approach, *e.g.* that contact area difference can be linked to the surface curvature.

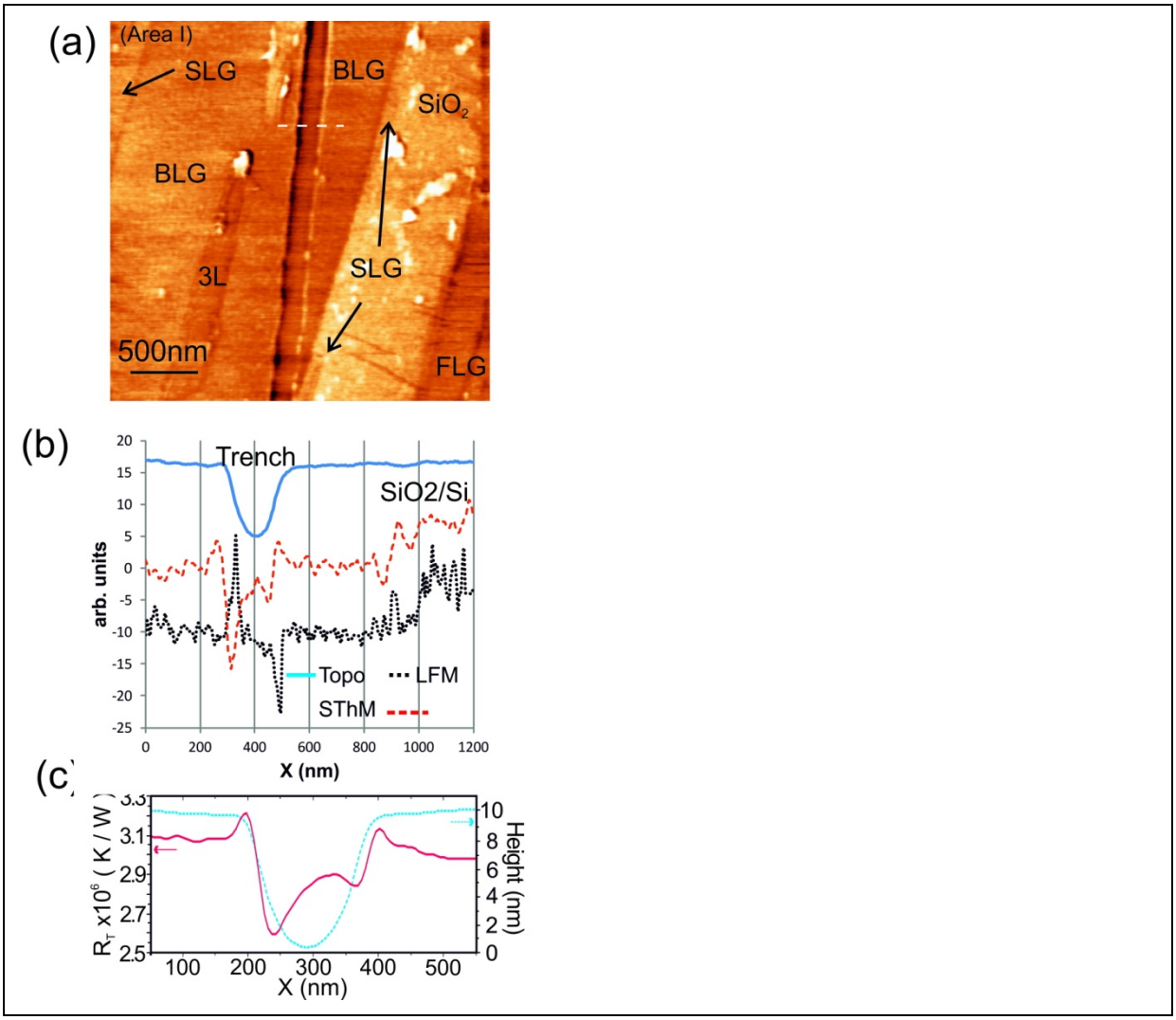

Figure 2 Imaging of heat transport in suspended graphene. **(a)** SThM thermal image (SThM map) of a zoom-in of graphene sample (dotted square in Fig. 1c) at a constant heating power. Lighter colour corresponds to higher temperature of the probe, and,correspondingly, a higher thermal resistance of the contact and a lower local heat conductance of the sample; the span of thermal contrast on the images corresponds to a probe temperature change of 0.4^{o} C. **(b)** Raw topography, SThM and lateral force (friction) microscopy LFM profiles acquired along the dashed line in (a). With the exception of SThM tip contact with trench edges (indicated by spikes in LFM signal), in the central area of the trench, LFM shows similar or slightly lower friction, suggesting no increase in the tip-surface contact area. **(c)** Topography profile (blue curve, right axis) and low noise averaged thermal resistance profile (red curve, left axis) averaged along the trench of bi-layer graphene suspended over the trench. Lower thermal resistance indicates an increase of the heat conductance of graphene with ballistic thermal phonons propagating from the area of the contact along the trench and towards edges of the trench.

As nanoscale thermal probe-sample dimensions L approach and fall below the MFP of phonons l, consideration of the ballistic regime in the analysis of these data becomes essential. The theoretical analysis also predicts that thermal resistance[32, 33] of the contact area depends on Knudsen number $Kn = l/L$. Low Knudsen numbers $Kn << 1$ correspond to the diffusive transport and high $Kn >> 1$ correspond to ballistic transport. It is shown elsewhere[34-36] that in the transition regime a good approximation for thermal resistance will be a summation of the diffusive and ballistic thermal resistances that would lead to the corresponding increase in total thermal resistance of tip-surface contact with respect to the thermal resistance in a diffusive heat transport approximation by a factor of $[1+ (8/3\pi)Kn]$.[33] Whereas the heat transfer within SThM probe (with l in SiO_2 and Pd much less than 50 nm probe size) and in the graphene film on the substrate (as shown in the theoretical analysis below) are well described by the diffusive approximation, the heat transfer in the suspended graphene layer is well within the ballistic regime, and this leads to a corresponding exaggeration of measured thermal resistance R_G.

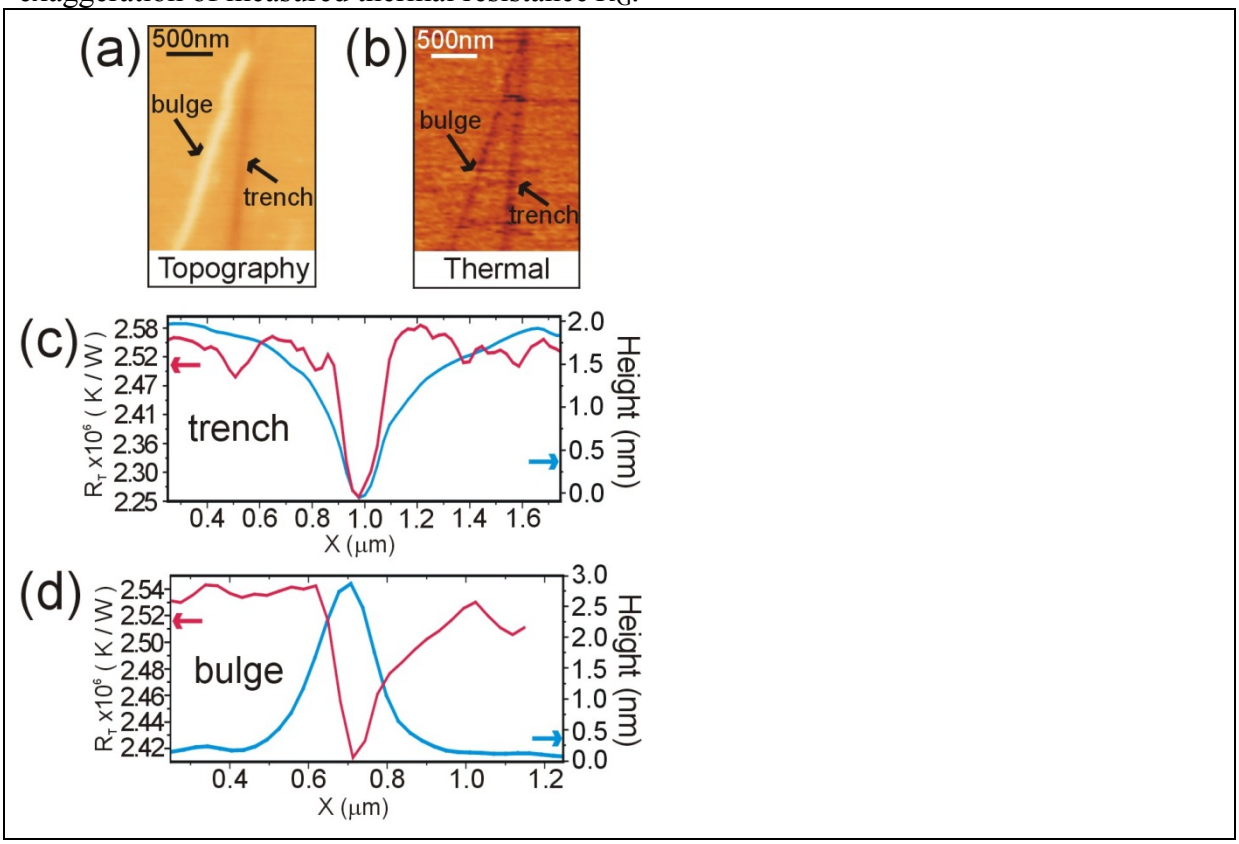

Figure 3 (**a)** AFM topography and (**b)** thermal image of a linearly extended graphene bulge in suapended MLG out of contact with the surface. Topography and SThM profiles of the trench **(c)** and bulge **(d)** areas (blue curves – topography, red curves- SThM profiles, with axis as above) show that corrugations of similar height (2-3 nm) but opposite curvature have similar thermal resistance changes**.** It is to be noted that both show a clear increase of thermal conductance for suspended graphene (in bulge and trench alike), independent of the sign of surface curvatureswhich allows us to rule out possible artefacts of contact area difference in thermal SThM measurements.

SThM measurements of thermal resistance of supported graphene layers of various thicknesses show absolute values of thermal resistances R_C decreasing from $3.08\text{x}10^6 \pm 3\text{x}10^4$ K/W for SLG, to $2.98\text{x}10^6 \pm 3\text{x}10^4$ K/W, $2.76\text{x}10^6 \pm 3\text{x}10^4$ K/W, to $2.58\text{x}10^6 \pm 3\text{x}10^4$ K/W for 3, 5 and 17-layer graphene, respectively, see Fig. 4a. These measurements allowed us to calculate using Eq. 2 the values of intrinsic graphene sheet thermal resistance for SLG $R_{G(SLG)} = 7.8\text{x}10^5 \pm 6\text{x}10^4$ K/W and $R_{G(3L)} = 3.8\text{x}10^5 \pm 6\text{x}10^4$ K/W. This puts thermal conductance of a 3-layer supported graphene, per single graphene layer, at approximately 68% of the SLG thermal conductance, that can be compared with measurements by Raman approaches[7].

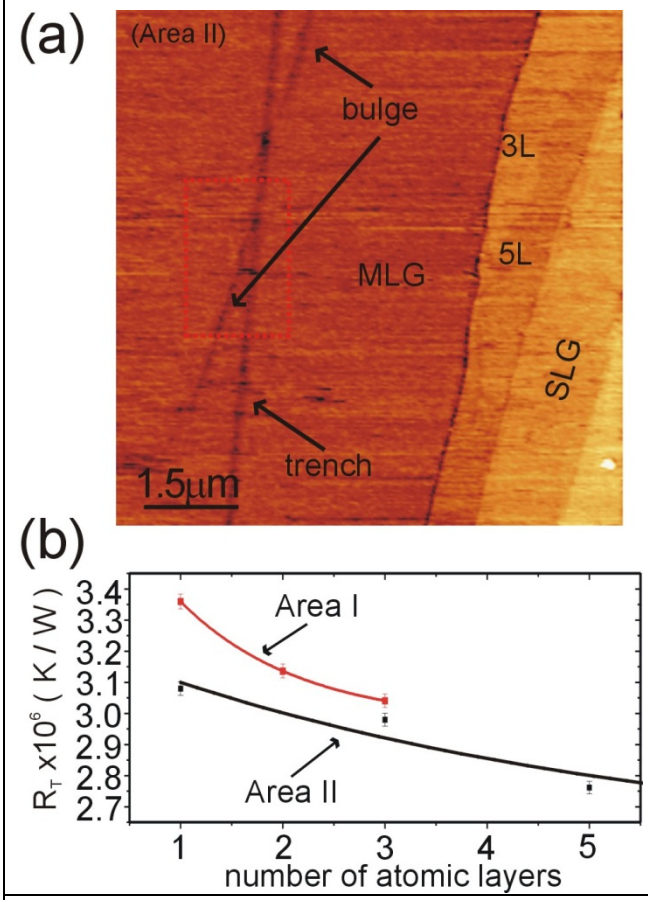

Figure 4 Heat transport in supported graphene. **(a)** SThM image of graphene of various thickness, taken in constant power mode. Values of contact thermal resistances R_c for the different areas of the sample are: SLG – $R_{c(SLG)} = 3.08\text{x}10^6 \pm 3\text{x}10^4$ K/W, 3 layers graphene - $R_{c(3L)} = 2.98\text{x}10^6 \pm 3\text{x}10^4$ K/W, 5 layers graphene - $R_{c(5L)} = 2.76\text{x}10^6 \pm 3\text{x}10^4$ K/W, and for 17 layers graphene (MLG) – $R_{c(MLG)} = 2.58\text{x}10^6 \pm 3\text{x}10^4$ K/W. **(b)** Measured contact thermal resistance as a function of the number of graphene layers (error bars represent STD of pixel based measurements taken along the line parallel to the boundary). Whereas the reduction in the thermal resistance with the increased number of layers was consistently observed, absolute values of measured thermal resistance were different between the flake main body (Area II) and its perifery (Area I), that may reflect the degree of adhesion between the flake and the supporting substrate in the particular area .

It is possible to approximate the two-dimensional thermal conductivity of graphene layer lying on a rough substrate as

$$\kappa = l\,(a_{ZA}/\lambda_{ZA} + a_{LA}/\lambda_{LA} + a_{TA}/\lambda_{TA})\;\pi N k_B(k_B T/h), \qquad [3]$$

where $\pi k_B(k_B T/h)$ is the quantum unit of heat conductance,[37,38] k_B and h are Boltzmann's and Planck's constants, N is the number of layers in the flake, $l = 1/n_i a$ is the energy/mode-independent elastic mean free path of phonons limited by scattering from the regions of typical size a tightly clamped to the tops of the 'hills' of SiO_2 surface with areal density n_i, and λ's are thermal wavelengths of ZA, LA, and TA phonons[10], λ_{ZA}~1nm, λ_{LA}~λ_{TA}~*2nm,* and a_{ZA}≈4.5, a_{LA}≈a_{TA}≈7.

The diffusion coefficient, D, for phonons travelling with velocity v and MFP l is $D = \frac{1}{2}vl$. Here we assume that phonon scattering occurs from the 'hill' tops on SiO_2 surface, with area density n_i and cross-section $a > \lambda$ determined by the local curvature, where λ is the wavelength of thermal phonons. Phonon wavelength is linked with phonon energy ε using

linear dispersion relationship for longitudinal (LA) and transverse (TA) phonons - $\lambda_{\varepsilon(LA,TA)}=v_{(LA,TA)}h/\varepsilon$, and quadratic relationship for the flexural (ZA) phonons, $\lambda_{za}=h(\alpha/\varepsilon)^{1/2}$, where α is the dispersion coefficient[10]. The contribution of one lattice mode towards two-dimensional heat conductivity can be expressed as

$$\kappa=\int D(\varepsilon)v(\varepsilon)\varepsilon k_B(\partial f/\partial\varepsilon)(-\varepsilon/k_BT)d\varepsilon, \quad [4]$$

where $f(\varepsilon)$ is the distribution function of phonons, $v(\varepsilon)_{ZA}=\pi/(h^2\alpha)$ and $v(\varepsilon)_{LA,TA}=2\pi\varepsilon/(hv_{LA.TA})^2$ are the 2D densities of states of phonons, namely, ZA, LA and TA phonons. Substituting values for D and integrating, obtained for BLG, $\kappa_{ZA}\sim4.5\pi k_B(k_BT/h)l\lambda_{T(ZA)}$ per layer and $\kappa_{LA,TA}\sim7\pi k_B(k_BT/h)/\lambda_{T(LA,TA)}$.

For two circuits consisting of a probe-tip (with radius less than l) that touches graphene in (a) the part supported by SiO_2 and (b) in the middle of suspended part with width w, and the thermal resistance of the tip-graphene junction R_j, the total heat resistance of the circuit has the form

$$R_{Ga}=R_j+\kappa^{-1}ln(L_s/l) \text{ and } R_{Gb}=R_j+\kappa^{-1}ln(L_s/w), \text{ for } L_s>w>l, \quad [5]$$

where L_s is the length at which heat gets transferred from graphene into the underlying substrate. By comparing the difference $R_{Ga}- R_{Gb}=\kappa^{-1}ln(w/l)$ to the measured values we find $l\sim100$nm. This value compares well with the typical width of temperature transitions in the supported graphene that we observed in the vicinity of the trench edge (Fig. 2b) and provides an estimate for characteristic length scale for heat transfer phenomena in graphene nanostructures.

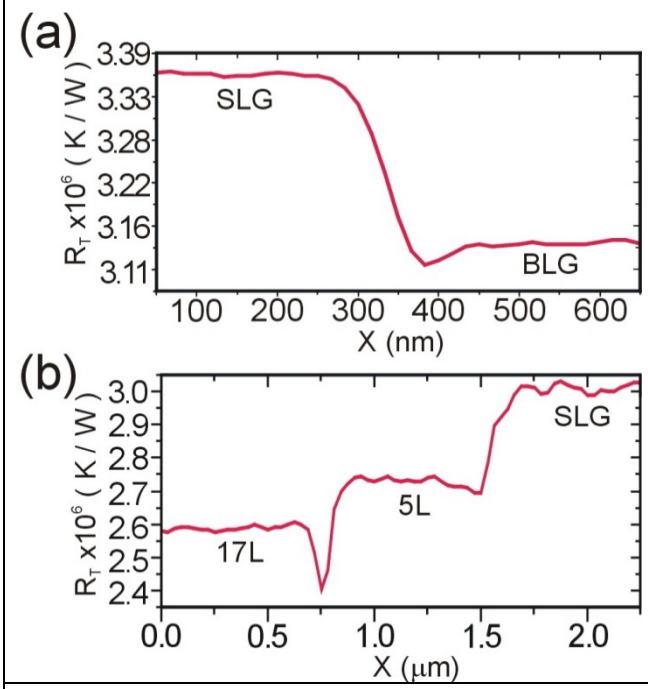

Figure 5 (a) 1D profile of the thermal resistance across the boundary between SLG and BLG layers. The width of transition area for thermal resistance is ~50 nm, whichis well below the average MFP of thermal phonons in suspended graphene (**b)** 1D profile of the thermal resitance across boundaries between SLG, five layers (5L), and 17 layers (MLG) of supported graphene.

Finally, one can see that nanoscale thermal mapping of border regions between supported graphene layers of different thicknesses (Fig. 5a, b) show that the thermal transition region

has a width of 50 to 100 nm. Given 50 nm resolution of our method, such length scale suggests that the value for MFP of phonons in graphene on the support is below 100 nm, therefore verifying the reason for lower thermal conductivity in supported graphene,[6] and our theoretical estimates for the mean free path.

In conclusion, we have explored thermal transport in single to few-layer graphene using a nanoscale thermal probe with true nanoscale resolution of a few tens of nanometres. We have observed higher thermal conductance due to ballistic phonons propagating in the 180 nm wide suspended graphene sheet, compared to the same sheet resting on the substrate. We found that thermal conductance of a 3-layer supported graphene, per single graphene layer, was at approximately 68% of the SLG thermal conductance. Direct imaging of spatial distribution of heat transport in graphene nanostructures indicated that the MFP of thermal phonons of supported graphene is below 100 nm. We believe that this advancement opens new ground for nanoscale exploration of heat transport and heat management in graphene-based and other nanoelectronic devices.

Acknowledgement. This work was supported in part by the UK Engineering and Physical Sciences Research Council (EPSRC) under grant awards EP/G015570/1, EP/G06556X/1 (EPSRC-NSF), EP/G017301/1, and the European Commission awards FUNPROBE and GRENADA.

References

1. Novoselov, K. S.; Geim, A. K.; Morozov, S. V.; Jiang, D.; Zhang, Y.; Dubonos, S. V.; Grigorieva, I. V.; Firsov, A. A. *Science* **2004,** 306, (5696), 666-669.
2. Gass, M. H.; Bangert, U.; Bleloch, A. L.; Wang, P.; Nair, R. R.; Geim, A. K. *Nat Nano* **2008,** 3, (11), 676-681.
3. Novoselov, K. S.; Geim, A. K.; Morozov, S. V.; Jiang, D.; Katsnelson, M. I.; Grigorieva, I. V.; Dubonos, S. V.; Firsov, A. A. *Nature* **2005,** 438, (7065), 197-200.
4. Balandin, A. A.; Ghosh, S.; Bao, W.; Calizo, I.; Teweldebrhan, D.; Miao, F.; Lau, C. N. *Nano Letters* **2008,** 8, (3), 902-907.
5. Nika, D. L.; Ghosh, S.; Pokatilov, E. P.; Balandin, A. A. *Applied Physics Letters* **2009,** 94, (20), 203103-3.
6. Cai, W.; Moore, A. L.; Zhu, Y.; Li, X.; Chen, S.; Shi, L.; Ruoff, R. S. *Nano Letters* **2010,** 10, (5), 1645-1651.
7. Ghosh, S.; Bao, W.; Nika, D. L.; Subrina, S.; Pokatilov, E. P.; Lau, C. N.; Balandin, A. A. *Nat Mater* **2010,** 9, (7), 555-558.
8. Ghosh, S.; Calizo, I.; Teweldebrhan, D.; Pokatilov, E. P.; Nika, D. L.; Balandin, A. A.; Bao, W.; Miao, F.; Lau, C. N. *Applied Physics Letters* **2008,** 92, (15), 151911-3.
9. Seol, J. H.; Jo, I.; Moore, A. L.; Lindsay, L.; Aitken, Z. H.; Pettes, M. T.; Li, X.; Yao, Z.; Huang, R.; Broido, D.; Mingo, N.; Ruoff, R. S.; Shi, L. *Science* **2010,** 328, (5975), 213-216.
10. Balandin, A. A. *Nat. Mater.* **2011,** 10, (8), 569-581.
11. Kim, P.; Shi, L.; Majumdar, A.; McEuen, P. L. *Physical Review Letters* **2001,** 87, (21), 215502.
12. Yu, C.; Shi, L.; Yao, Z.; Li, D.; Majumdar, A. *Nano Letters* **2005,** 5, (9), 1842-1846.
13. Shi, L.; Majumdar, A. *Journal of Heat Transfer-Transactions of the Asme* **2002,** 124, (2), 329-337.
14. Li, D. Y.; Wu, Y. Y.; Kim, P.; Shi, L.; Yang, P. D.; Majumdar, A. *Applied Physics Letters* **2003,** 83, (14), 2934-2936.
15. Berber, S.; Kwon, Y.-K.; Tom; aacute; nek, D. *Physical Review Letters* **2000,** 84, (20), 4613.
16. Klemens, P. G. *Int. J. Thermophys.* **2001,** 22, (1), 265-275.
17. Qiu, B.; Ruan, X., Mechanism of Thermal Conductivity Reduction from Suspended to Supported Graphene: a Qunatitative Spectral Analysis of Phonon Scattering. In *ASME 2011 International Mechanical Engineering Congress, IMECE2011*, Denver, Colorado, USA, 2011; p 62963.
18. Balandin, A. A.; Ghosh, S.; Bao, W. Z.; Calizo, I.; Teweldebrhan, D.; Miao, F.; Lau, C. N. *Nano Letters* **2008,** 8, (3), 902-907.
19. Minkel, J. *Scientific American* **2007**.
20. Ferrari, A. C.; Meyer, J. C.; Scardaci, V.; Casiraghi, C.; Lazzeri, M.; Mauri, F.; Piscanec, S.; Jiang, D.; Novoselov, K. S.; Roth, S.; Geim, A. K. *Physical Review Letters* **2006,** 97, (18), 187401.

21. Blake, P.; Hill, E. W.; Neto, A. H. C.; Novoselov, K. S.; Jiang, D.; Yang, R.; Booth, T. J.; Geim, A. K. *Applied Physics Letters* **2007,** 91, (6), 063124-3.
22. Nair, R. R.; Blake, P.; Grigorenko, A. N.; Novoselov, K. S.; Booth, T. J.; Stauber, T.; Peres, N. M. R.; Geim, A. K. *Science* **2008,** 320, (5881), 1308.
23. McGuigan, A. P.; Huey, B. D.; Briggs, G. A. D.; Kolosov, O. V.; Tsukahara, Y.; Yanaka, M. *Applied Physics Letters* **2002,** 80, (7), 1180-1182.
24. Rosamond, M. C.; Gallant, A. J.; Petty, M. C.; Kolosov, O.; Zeze, D. A. *Adv. Mater.* **2011,** 23, (43), 5039-5044.
25. Majumdar, A. *Annu. Rev. Mater. Sci.* **1999,** 29, 505-585.
26. Hinz, M.; Marti, O.; Gotsmann, B.; Lantz, M. A.; Durig, U. *Applied Physics Letters* **2008,** 92, (4), 043122-3.
27. Mills, G.; Zhou, H.; Midha, A.; Donaldson, L.; Weaver, J. M. R. *Applied Physics Letters* **1998,** 72, (22), 2900-2902.
28. Dobson, P. S.; Weaver, J. M. R.; Mills, G.; Ieee, New methods for calibrated Scanning Thermal Microscopy (SThM). In *2007 Ieee Sensors, Vols 1-3*, Ieee: New York, 2007; pp 708-711.
29. Ahmad, M.; Hayne, M.; Zhuang, Q. D.; Kolosov, O.; Nuytten, T.; Moshchalkov, V. V.; Dinelli, F. *Journal of Physics: D Applied Physics* **2010,** 43, (6), 065402-065402.
30. Koh, Y. K.; Bae, M.-H.; Cahill, D. G.; Pop, E. *Nano Letters* **2010,** 10, (11), 4363-4368.
31. Shi, L.; Plyasunov, S.; Bachtold, A.; McEuen, P. L.; Majumdar, A. *Applied Physics Letters* **2000,** 77, (26), 4295-4297.
32. Puyoo, E.; Grauby, S.; Rampnoux, J. M.; Rouviere, E.; Dilhaire, S. *J. Appl. Phys.* **2011,** 109, (2), 9.
33. Prasher, R. *Nano Lett.* **2005,** 5, (11), 2155-2159.
34. Ordonez-Miranda, J.; Yang, R. G.; Alvarado-Gil, J. J. *J. Appl. Phys.* **2011,** 109, (8), 8.
35. Chen, G. *Phys. Rev. Lett.* **2001,** 86, (11), 2297-2300.
36. Alvarez, F. X.; Jou, D. *Appl. Phys. Lett.* **2007,** 90, (8), 3.
37. Rego, L. G. C.; Kirczenow, G. *Physical Review Letters* **1998,** 81, (1), 232.
38. Kambili, A.; Fagas, G.; Falko, V. I.; Lambert, C. J. *Physical Review B* **1999,** 60, (23), 15593.